BIOCHEMISTRY
including biophysical chemistry & molecular biology

Article

pubs.acs.org/biochemistry

Structural Studies of AntD: An *N*-Acyltransferase Involved in the Biosynthesis of D-Anthrose

Rachel L. Kubiak and Hazel M. Holden*

Department of Biochemistry, University of Wisconsin, Madison, Wisconsin 53706, United States

ABSTRACT: The unusual dideoxy sugar D-anthrose has been identified as an important component in the endospores of infectious agents such as *Bacillus anthracis* and *Bacillus cereus*. Specifically, it is the terminal sugar on the bacterium's exosporium, and it provides a point of interaction between the spore and the host. The biosynthesis of D-anthrose involves numerous steps starting from α-D-glucose 1-phosphate. Here we present a combined structural and functional investigation of AntD from *B. cereus*. This enzyme plays a key role in D-anthrose biosynthesis by catalyzing the acylation of the C-4″ amino group of dTDP-4-amino-4,6-dideoxyglucose using 3-hydroxy-3-methylbutyryl-CoA as the acyl donor. For this investigation, two ternary complexes of AntD were determined to 1.8 Å resolution: one in which the protein contained bound β-hydroxybutyryl-CoA and dTDP and the second with CoA and dTDP-4-amino-4,6-dideoxyglucose. On the basis of these high-resolution structures, it was shown that the side chain of Asp 94 lies within hydrogen bonding distance of the sugar C-4″ amino group, and the side chain of Ser 84 resides near the carbonyl oxygen of β-hydroxybutyryl-CoA. To test the roles of these residues in the catalytic mechanism of AntD, various site-directed mutant proteins were prepared and subjected to kinetic and structural analyses. The D94A and D94N mutant proteins demonstrated enzymatic activity, albeit with significantly reduced catalytic efficiencies. The S84A mutant protein showed an approximate 10-fold decrease in activity. Interestingly, the S84C and S84T mutant proteins were both active but demonstrated substrate inhibition. The three-dimensional structures of all of the mutant proteins were nearly identical to that of the wild-type enzyme, indicating that the changes in their kinetic parameters were not due to major conformational changes. Taken together, these data suggest that Asp 94 is important for substrate binding, but probably does not function as an enzymatic base, and that Ser 84 most likely plays a role in the formation of an oxyanion hole.

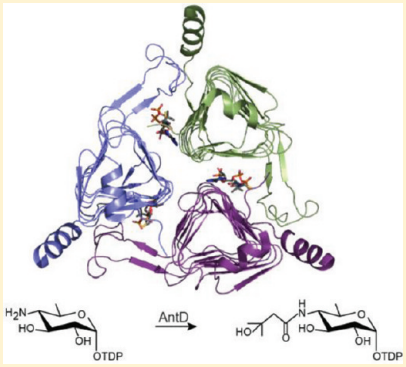

Bacillus anthracis, the causative agent of anthrax, is a ubiquitous soil-dwelling Gram-positive bacterium that typically infects plant-eating mammals such as cattle, sheep, and goats. Like other members of the *Bacillus* genus, it produces endospores that can withstand extremely harsh environmental conditions over extended periods of time.[1] It is the entry of these endospores into the host that leads to the development of anthrax.[2] The outermost layer of the spore is termed the exosporium, and it functions both as a permeability barrier and as a source of antigens.[3,4] The exosporium consists of approximately 50% protein, 20% lipid, 20% carbohydrate, and 10% other components.[5] Recent studies have suggested that the exosporium is composed of approximately 20 different proteins.[3,6,7] One of these is a glycoprotein referred to as Bc1A.[8−10] Two oligosaccharides are attached to Bc1A, one of which contains an intriguing dideoxy sugar termed D-anthrose [2-*O*-methyl-4-(3-hydroxy-3-methylbutamido)-4,6-dideoxy-D-glucose].[10,11] It is this anthrose-containing species that is serving as a promising target for the development of specific and sensitive detection devices.[12] Originally thought to be confined only to *B. anthracis*, D-anthrose has now been observed in related *Bacillus cereus* and *Bacillus thuringiensis* strains.[11] It has also been reported in the oligosaccharides of certain *Pseudomonas*, *Shewanella*, and *Mycobacterium* organisms.[13,14]

The proposed pathway for the biosynthesis of D-anthrose, starting from dTDP-4-keto-6-deoxy-D-glucose, is shown in Scheme 1.[15] In the first step, the C-4″ keto group is aminated by the action of AntC, a PLP-dependent enzyme. AntD catalyzes the next step, the transfer of an acyl group from 3-hydroxy-3-methylbutyryl-CoA to the C-4″ amino group of the hexose. The amino acid sequence identity is 99% between the versions of AntD from *B. anthracis* and *B. cereus*. The identity of the enzyme that catalyzes the final O-methylation reaction shown in Scheme 1 is unknown at present.

On the basis of its amino acid sequence, it is clear that AntD belongs to the left-handed β-helix (LBH) superfamily of *N*-acyltransferases.[16] Members of the family contain repeated isoleucine-rich hexapeptide motifs and rare left-handed cross-over connections.[16] In recent years, a number of these enzymes that function specifically on nucleotide-linked sugars have been structurally characterized.[17−20] Whereas they all adopt left-handed β-helical structures, their active sites are considerably different, and they accommodate their nucleotide-linked sugars in remarkably different orientations. In some family members, it is thought that an active site histidine serves as a catalytic base

Received: November 1, 2011
Revised: January 4, 2012
Published: January 4, 2012

Scheme 1

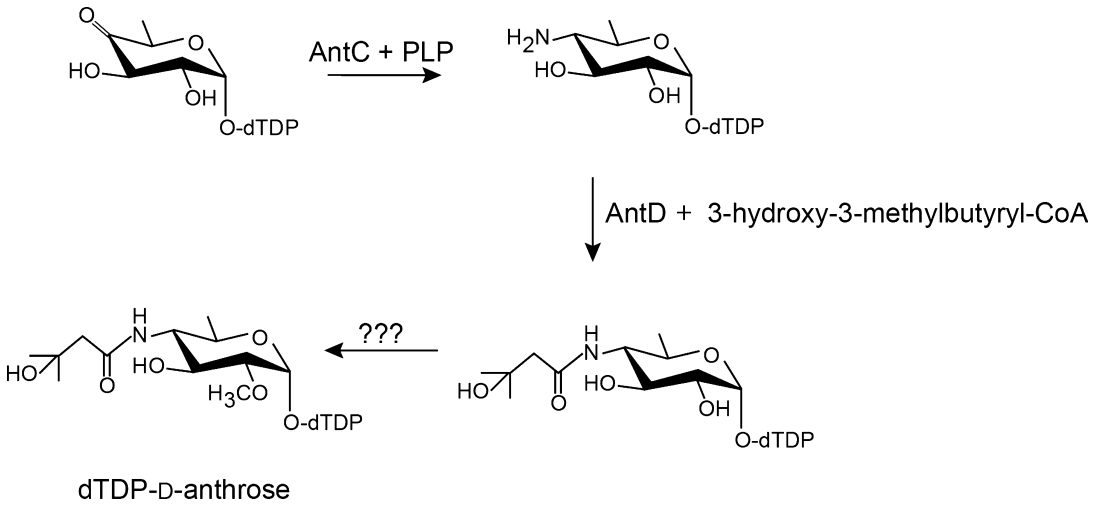

to remove a proton from the sugar amino group.[17,18] In others, it has been proposed that the sulfur of CoA ultimately functions as the proton acceptor required for catalysis.[19,20]

For the X-ray analysis presented here, we determined two high-resolution structures of AntD from *B. cereus*: one in complex with CoA and its dTDP-sugar substrate and the other with bound *β*-hydroxybutyryl-CoA and dTDP. In addition, we probed the roles of Ser 84 and Asp 94 in catalysis via site-directed mutagenesis, kinetic experiments, and structural analyses. Taken together, these data suggest that catalysis by AntD most likely occurs via a substrate-assisted mechanism.

MATERIALS AND METHODS

Cloning, Expression, and Purification. The *AntD* gene was amplified via PCR from *B. cereus* SJ1 (NRRL B-59452) genomic DNA using the forward primer 5′-AAA*CATATG*AATAGTTTTTATAGTCAAG-3′ and the reverse primer 5′-AAA*CTCGAG*TCAAGAGTTCATACTT-3′, which added *Nde*I and *Xho*I cloning sites, respectively. The purified PCR product was subsequently A-tailed and ligated into a pGEM-T vector (Promega) for screening and sequencing. A pGEM-T-*AntD* vector construct of the correct sequence was then digested appropriately, and the gene was ligated into a pET28JT vector[21] for the production of protein with a TEV protease cleavable N-terminal hexahistidine tag.

The pET28JT-*AntD* plasmid was used to transform Rosetta 2 (DE3) *Escherichia coli* cells (Novagen). Cultures were grown with shaking at 37 °C in Luria-Bertani broth supplemented with kanamycin and chloramphenicol until optical densities of 0.8 were reached at 600 nm. The flasks were then cooled to 16 °C, and the cells were subsequently induced with the addition of 1 mM isopropyl *β*-D-1-thiogalactoside. Protein expression was allowed to occur at 16 °C for 18 h following induction. AntD was purified by standard procedures using Ni-nitrilotriacetic acid resin (Qiagen). The purified protein was dialyzed against 10 mM HEPES (pH 7.5) and 100 mM NaCl, concentrated to ∼20 mg/mL, and flash-frozen in liquid nitrogen.

Activity Assay. The natural substrate for AntD is 3-hydroxy-3-methylbutyryl-CoA. This compound is commercially unavailable. However, *β*-hydroxybutyryl-CoA can be obtained, and it differs from the natural substrate by one methyl group (Scheme 2). Previous studies have shown that AntD from

Scheme 2

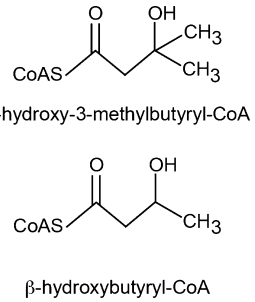

B. anthracis can use this alternative substrate.[15] To verify that AntD from *B. cereus* can also function on *β*-hydroxybutyryl-CoA, reaction mixtures were set up to contain 50 mM HEPES (pH 7.5), 0.5 mM dTDP-4-amino-4,6-dideoxy-D-glucose, 0.5 mM *β*-hydroxybutyryl-CoA, and 1 mg/mL AntD. The required dTDP-4-amino-4,6-dideoxy-D-glucose was synthesized according to previously published procedures.[22] The reaction mixtures were incubated at 24 °C for 3 h, with samples taken at 0 and 3 h time points. Samples were passed through a 10 kDa cutoff filter (Amicon) to remove the enzymes, and the filtrates were diluted 1:9 with water.

The reaction mixtures were analyzed via an ÄKTA Purifier high-performance liquid chromatography (HPLC) system (GE Healthcare) equipped with a Resource-Q 1 mL anion exchange column (GE Healthcare). Using a 20 mL linear gradient from 0 to 600 mM ammonium bicarbonate (pH 8.5) run at a rate of 2 mL/min, a new peak was seen eluting in the 3 h sample. The product corresponding to this peak was collected, and its identity as a *β*-hydroxybutyrylated sugar was confirmed by ESI mass spectrometry (Mass Spectrometry/Proteomic Facility at the University of Wisconsin) as shown in Figure 1 with a parent ion at m/z 632.

Crystallization of AntD. Crystallization conditions were initially surveyed by the hanging drop method of vapor diffusion using a sparse matrix screen developed in the laboratory. The protein concentration was 15 mg/mL, and the sample contained 10 mM dTDP and 10 mM CoA. X-ray diffraction quality crystals of the N-terminally His-tagged protein were grown by mixing in a 1:1 ratio the enzyme solution with 25% pentaerythritol ethoxylate (3:4 EO:OH ratio) and 2%

dx.doi.org/10.1021/bi201650c | *Biochemistry* 2012, 51, 867−878

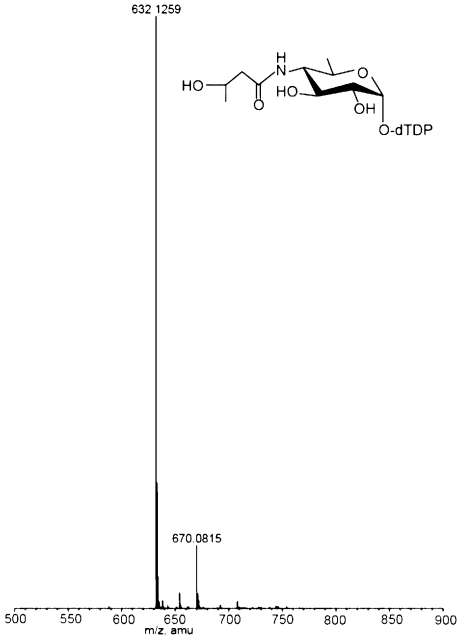

Figure 1. Mass spectrum of the AntD product. The parent ion at m/z 632 corresponds to the dTDP-linked β-hydroxybutyrylated sugar.

2-propanol at pH 6.0. These crystals belonged to the space group $P4_1$ with the following unit cell dimensions: $a = b = 72.3$ Å, and $c = 139.6$ Å. The asymmetric unit contained three monomers.

Structural Analysis of AntD. The initial structure of AntD was determined by multiple isomorphous replacement with two heavy atom derivatives. The crystals were first transferred to a synthetic mother liquor containing 26% pentaerythritol ethoxylate (3:4 EO:OH ratio), 10% poly(ethylene glycol) 3400, 2% 2-propanol, 200 mM NaCl, and 10 mM dTDP at pH 8.0 for at least 24 h. They were subsequently soaked in solutions containing either 0.7 mM methylmercuric acetate or 29 mM trimethyllead acetate for 2 h or 9 days, respectively. X-ray data were measured at 4 °C with a Bruker AXS HI-STAR area detector system equipped with Supper mirrors. The X-ray source was Cu Kα radiation from a Rigaku RU200 X-ray generator operated at 50 kV and 90 mA. Five mercury and five lead binding sites were identified with SOLVE.[23] Solvent flattening with RESOLVE[24] generated an interpretable electron density map, and a preliminary model of the enzyme was constructed using Coot.[25]

For higher-resolution X-ray data sets, crystals grown in the presence of 10 mM dTDP and 10 mM CoA were soaked for several hours in various synthetic mother liquors containing either 10 mM dTDP-4-amino-4,6-dideoxy-D-glucose and 10 mM CoA or 10 mM dTDP and 30 mM β-hydroxybutyryl-CoA, in addition to 26% pentaerythritol ethoxylate (3:4 EO:OH ratio), 10% poly(ethylene glycol) 3400, 2% 2-propanol, and 200 mM NaCl (pH 8.0). High-resolution X-ray data sets were collected at 100 K with a Bruker AXS Platinum 135 CCD detector equipped with Montel optics and controlled by the Proteum software suite (Bruker AXS Inc.). These data sets were processed with SAINT version 7.06A (Bruker AXS Inc.) and internally scaled with SADABS version 2005/1 (Bruker AXS Inc.). Relevant X-ray data collection statistics are listed in Table 1. Both ternary complex models were constructed using Coot and refined with REFMAC.[26] Refinement statistics are listed in Table 2.

Table 1. X-ray Data Collection Statistics[a]

	wild-type enzyme/ no bound ligands	methylmercuric acetate	trimethyllead acetate	enzyme/CoA/ dTDP-sugar	enzyme/acyl-CoA/dTDP	D94N/CoA/ dTDP	D94A/CoA/ dTDP	S84A/CoA/ dTDP-sugar	S84T/CoA/ dTDP	S84C/CoA/ dTDP-sugar
resolution limits (Å)	30.0–2.7 (2.8–2.7)	30.0–2.7 (2.8–2.7)	30.0–2.7 (2.8–2.7)	30.0–1.8 (1.9–1.8)	30.0–1.8 (1.9–1.8)	30.0–2.3 (2.4–2.3)	30.0–2.5 (2.6–2.5)	30.0–2.2 (2.3–2.2)	30.0–1.9 (2.0–1.9)	30.0–1.9 (2.0–1.9)
no. of independent reflections	18559 (1700)	19034 (1803)	19972 (1946)	57751 (7460)	60265 (7806)	29979 (3122)	22486 (2201)	33434 (3509)	52346 (6891)	52194 (7076)
completeness (%)	93.9 (81.1)	96.3 (88.9)	95.7 (85.2)	90.9 (78.0)	94.9 (89.1)	97.5 (92.8)	94.4 (80.7)	95.3 (86.7)	96.7 (89.4)	97.3 (92.1)
redundancy	2.4 (1.2)	2.4 (1.3)	2.6 (1.4)	3.7 (1.6)	4.3 (2.3)	4.4 (2.7)	4.0 (1.4)	4.1 (2.0)	4.3 (2.0)	4.1 (2.3)
avg I/avg $\sigma(I)$	5.9 (1.9)	8.1 (2.5)	7.3 (2.4)	11.8 (1.6)	14.7 (2.4)	8.2 (2.7)	5.9 (1.6)	14.4 (3.1)	8.8 (2.5)	8.9 (2.8)
R_{sym} (%)[b]	11.2 (25.4)	8.0 (21.5)	9.8 (24.9)	6.2 (38.3)	5.4 (29.0)	10.0 (31.1)	15.1 (38.0)	5.5 (18.9)	8.4 (28.9)	9.1 (29.1)

[a]Statistics for the highest-resolution bin are in parentheses. [b]$R_{sym} = (\sum|I - \bar{I}|/I) \times 100$.

dx.doi.org/10.1021/bi201650c | Biochemistry 2012, 51, 867–878

Table 2. Refinement Statistics

	enzyme/CoA/dTDP-sugar	enzyme/acyl-CoA/dTDP	D94N/CoA/dTDP	D94A/CoA/dTDP	S84A/CoA/dTDP-sugar	S84T/CoA/dTDP	S84C/CoA/dTDP-sugar
space group	$P4_1$	$P4_1$	$P4_1$	$P4_1$	$P4_1$	$P4_1$	$P4_1$
unit cell dimensions (Å)	$a = b = 71.1$, $c = 138.2$	$a = b = 70.9$, $c = 138.6$	$a = b = 71.3$, $c = 138.2$	$a = b = 71.1$, $c = 137.7$	$a = b = 71.3$, $c = 138.4$	$a = b = 71.0$, $c = 138.9$	$a = b = 70.7$, $c = 138.7$
resolution limits (Å)	71.0−1.8	71.0−1.8	71.0−2.3	71.1−2.5	71.0−2.2	71.0−1.9	70.8−1.9
$R_{overall}$[a] (%)/no. of reflections	20.0/57719	18.1/60245	19.2/29957	20.0/22458	19.0/33423	18.0/52311	17.3/52146
$R_{working}$ (%)/no. of reflections	19.8/54826	17.8/57176	18.9/28459	19.6/21291	18.6/31748	17.7/49653	17.0/49516
R_{free} (%)/no. of reflections	24.5/2893	22.8/3069	25.9/1498	27.7/1167	25.2/1675	22.2/2658	22.0/2630
no. of protein atoms	4340	4386	4316	4312	4319	4448	4397
no. of heteroatoms	560[b]	665[c]	348[d]	281[e]	401[f]	522[g]	595[h]
average B value (Å^2)							
protein atoms	27.2	24.7	35.4	28.3	30.2	20.3	18.0
ligands	27.7	31.1	48.8	41.1	31.5	22.7	22.3
solvent	31.8	32.5	32.9	19.7	28.4	25.4	23.6
weighted rmsd from ideality							
bond lengths (Å)	0.01	0.01	0.01	0.01	0.01	0.01	0.01
bond angles (deg)	2.3	2.3	2.3	2.2	2.2	2.4	2.4
general planes (Å)	0.009	0.009	0.009	0.009	0.010	0.011	0.009

[a] $R = (\sum|F_o - F_c|/\sum|F_o|) \times 100$, where F_o is the observed structure factor amplitude and F_c is the calculated structure factor amplitude. [b] These include one chloride ion, three CoA molecules, three dTDP-sugars, 298 waters, and three bicarbonate ions. [c] These include one chloride ion, three β-hydroxybutyryl-CoA molecules, three dTDP molecules, and 427 waters. [d] These include one chloride ion, three CoA molecules, three dTDP molecules, and 129 waters. [e] These include one chloride ion, three CoA molecules, three dTDP molecules, and 61 waters. [f] These include one chloride ion, three CoA molecules, three dTDP-sugars, and 151 waters. [g] These include one chloride ion, three CoA molecules, three dTDP molecules, 290 waters, and three bicarbonate ions. [h] These include one chloride ion, three CoA molecules, three dTDP-sugars, 333 waters, and three bicarbonate ions.

Production of Site-Directed Mutant Proteins. The D94N, D94A, S84A, S84T, and S84C mutations were introduced using methods described within the QuikChange site-directed mutagenesis kit (Stratagene). All mutant proteins were expressed, purified, and dialyzed in a manner identical to that for the wild-type enzyme. The mutant protein samples were concentrated to 15−20 mg/mL and flash-frozen in liquid nitrogen.

Activity assays were conducted for all mutant proteins. For each protein variant, the reaction mixture was identical to that previously described. Reactions were allowed to run for 3 h, and the samples were prepared and isolated via HPLC. As observed with wild-type AntD, a new peak was seen eluting for all of the mutant proteins. The product corresponding to this peak was collected, and the identity of the β-hydroxybutyrylated sugar was confirmed by ESI mass spectrometry with a parent ion at m/z 632.

Crystallization and Structural Analyses of the AntD Mutant Proteins. All mutant protein crystals were grown under conditions nearly identical to those used for the wild-type enzyme, and they belonged to the space group $P4_1$ and had similar unit cell dimensions.

X-ray data sets were collected for each of the mutant proteins and their structures solved by molecular replacement using the software package Phaser and the wild-type enzyme model as the search probe.[27] Relevant X-ray data collection and model refinement statistics are listed in Tables 1 and 2, respectively.

Measurement of Enzymatic Activity. *N*-Acyltransferase activity was monitored spectrophotometrically by following the increase in absorbance at 412 nm due to the reaction of the free sulfhydryl group of the CoASH product with 5,5′-dithiobis(2-nitrobenzoic acid). This reaction results in a disulfide interchange that leads to the formation of 5-thio-2-nitrobenzoic acid, which has a characteristic absorbance at 412 nm and an extinction coefficient of 14150 M^{-1} cm^{-1}. The use of this compound for quantification of free CoASH was first reported by Tomkins et al.,[28] and our assay method was similar to that described in ref 29. Reactions were continuously monitored with a Beckman DU 640B spectrophotometer. All reaction mixtures contained 50 mM HEPES (pH 7.5) and 5 mM 5,5′-dithiobis(2-nitrobenzoic acid) in addition to enzyme and substrates. The reactions were initiated by the addition of AntD to final concentrations of 0.1 μg/mL for the wild-type protein and 10 μg/mL for each of the D94N, D94A, S84A, S84T, and S84C mutant proteins.

Kinetic parameters for the wild-type enzyme were measured as follows. For determination of the K_m of the enzyme for dTDP-4-amino-4,6-dideoxy-D-glucose, the concentration of β-hydroxybutyryl-CoA was held constant at 4 mM while the dTDP-sugar concentration varied from 0.25 to 15 mM. For the determination of the K_m of the enzyme for β-hydroxybutyryl-CoA, the dTDP-sugar concentration was held constant at 10 mM while the β-hydroxybutyryl-CoA concentration varied from 0.075 to 4 mM.

To determine the K_m values of the mutant proteins for the dTDP-sugar substrate, the concentration of β-hydroxybutyryl-CoA was held constant at 5 mM. The D94A mutant protein required concentrations of the dTDP-sugar in the range of 2−50 mM, whereas the D94N mutant protein required dTDP-sugar concentrations ranging from 0.5 to 75 mM. For the S84A mutant protein, dTDP-sugar concentrations from 0.5 to 60 mM were

Table 3. Kinetic Parameters[a]

	K_m (mM)		k_{cat} (s^{-1})		k_{cat}/K_m (M^{-1} s^{-1})	
protein	dTDP-sugar	acyl-CoA	dTDP-sugar	acyl-CoA	dTDP-sugar	acyl-CoA
wild type	2.1 ± 0.2	0.67 ± 0.06	69.1 ± 2.7	69.4 ± 2.5	3.3×10^4	10.4×10^4
D94N	20.5 ± 1.4	2.33 ± 0.78	1.3 ± 0.1	1.9 ± 0.2	6.5×10	8.2×10^2
D94A	15.8 ± 2.9	0.32 ± 0.03	0.18 ± 0.01	0.59 ± 0.01	1.1×10	1.8×10^3
S84A	2.4 ± 0.5	0.15 ± 0.01	6.6 ± 0.3	5.8 ± 0.1	2.7×10^3	3.9×10^4
S84T	2.2 ± 1.2	nd[b]	4.8 ± 1.5	nd[b]	1.9×10^3	nd[b]
S84C	1.1 ± 0.4	nd[b]	5.5 ± 1.1	nd[b]	5.1×10^3	nd[b]

[a]Standard errors are reported. [b]Not determined.

used. Both the S84T and S84C mutant proteins required dTDP-sugar concentrations of 0.1−50 mM.

The K_m values of the mutant enzymes for β-hydroxybutyryl-CoA were also determined. The D94N mutant protein reactions were run with the dTDP-sugar concentration held constant at 120 mM while the β-hydroxybutyryl-CoA concentrations varied from 0.4 to 25 mM. The D94A mutant protein reactions were run with the dTDP-sugar concentration held constant at 80 mM while the β-hydroxybutyryl-CoA concentrations varied from 0.1 to 5.0 mM. In reactions using the S84A protein, the sugar concentration was held constant at 15 mM while the β-hydroxybutyryl-CoA concentration varied from 0.1 to 5.0 mM.

All data were fitted by initial velocity Michaelis−Menten kinetics to the equation $v = (V_{max}[S])/(K_m + [S])$, and k_{cat} values were calculated according to the equation $k_{cat} = V_{max}/[E_T]$. The kinetic data are listed in Table 3.

Both the S84C and S84T mutant enzymes demonstrated substrate inhibition at dTDP-sugar concentrations of >7.5 mM. As a consequence, it was not possible to determine the K_m of these mutant proteins for β-hydroxybutyryl-CoA. The reported K_m values of these two mutant proteins for the dTDP-sugar were determined using initial velocity kinetics and fitted to the equation $v = V_{max}[S]/K_m + [S](1 + [S]/K_i)$, where K_i is the inhibition constant (SigmaPlot version 8.0).

RESULTS AND DISCUSSION

Overall Structure of AntD. The first structure of AntD determined in this investigation was that of the protein in a complex with CoA and dTDP-4-amino-4,6-dideoxy-α-D-glucose. Note that each subunit of the trimeric enzyme contains 188 amino acid residues. The crystals diffracted to 1.8 Å resolution and belonged to space group $P4_1$ with a complete trimer in the asymmetric unit. Overall, the quality of the model was excellent with 87.2 and 12.8% of the ϕ and ψ values lying within the core and allowed regions of the Ramachandran plot, respectively.[30] The electron densities corresponding to two of the bound ligands in the asymmetric unit are presented in Figure 2a, and as can be seen, the conformations for both the CoA and nucleotide-linked sugar are unambiguous. The entire electron density map was well-ordered for all three polypeptide chains in the asymmetric unit, the exceptions being several regions at the N- and C-termini. Interestingly, there was a piece of "mysterious" electron density wedged between the dTDP-linked amino sugar ligand and the CoA in each subunit. Given the planar shape of the electron density and the fact that ammonium bicarbonate was used to prepare the dTDP-sugar, we assigned it to a bicarbonate ion with an occupancy of 0.5. In two of the site-directed mutant protein structures described below (S84T and S84C), the bicarbonate appeared to be at full occupancy, most likely due to differences in the amount of bicarbonate contamination in the dTDP-sugar preparations.

The polypeptide chain of each AntD subunit initiates with an extended region followed by a short α-helix defined by Gln 7−Lys 11 (Figure 2b). From there, the backbone folds into a left-handed β-helix of seven turns. The regularity of the β-helix is interrupted by an extended loop delineated by Ala 91 and Gly 116. This loop contains a two-stranded antiparallel β-sheet and a type I turn formed by Pro 107−Tyr 110. The loop extends toward another subunit in the trimer where it provides a binding platform for the CoA ligand and the dTDP-sugar substrate (Figure 2c). Following the β-helix motif, the polypeptide chain extends toward a second α-helix defined by Lys 174 to the C-terminus (Figure 2b). Pro 164, which abuts the adenine ring of CoA, adopts the *cis* conformation. The barrel of the β-helix is lined by five walls of hydrophobic residues, which are typically leucines, isoleucines, or valines. The AntD trimer has overall dimensions of 70 Å × 56 Å × 70 Å with the three active sites situated between subunits (Figure 2c). The buried surface area for each subunit in the trimer is ∼2700 $Å^2$.

Close-up views of the binding pockets for the cofactor and the nucleotide-linked sugar substrate are presented in panels a and b of Figure 3, respectively. The CoA moiety adopts a decidedly curved conformation such that the hydroxyl group of its pantothenate moiety lies within 2.7 Å of N-7 of its adenine ring. Only two side chains, Lys 151 and Lys 169, are directly involved in anchoring the cofactor to the protein, both of which interact with the pyrophosphoryl group of CoA. They are located on opposite sides of the pyrophosphoryl group and are contributed by two different subunits of the trimer. The backbone amide nitrogens of Ala 128 and Ala 146, along with the carbonyl oxygen of Ala 146, also participate in hydrogen bonding interactions with the cofactor. Whereas the pantothenate and β-mercaptoethylamine units of CoA are buried in the active site pocket, the pyrophosphoryl and ribose phosphate groups are solvent-exposed (Figure 3a). Numerous solvent molecules surround the cofactor.

The dTDP-4-amino-4,6-dideoxy-α-D-glucose substrate sits in the active site with its C-4″ amino group ∼2.9 Å from the sulfur of CoA (Figure 3b). The thymine ring, which participates in hydrogen bonding interactions with the backbone amide groups of Ser 3 and Asp 46, is sandwiched between the aromatic side chains of Phe 4 from one subunit and Tyr 31 from another. Both Arg 43 from one subunit and Ser 51 from the other lie within hydrogen bonding distance of the pyrophosphoryl moiety of the nucleotide-linked sugar. Strikingly, the hydroxyl groups of the hexose do not interact with protein side chains but rather with ordered water molecules or the bicarbonate ion. The amino group attached to C-4″ of the dTDP-sugar is positioned ∼3.1 Å from the carboxylate of Asp 94 and ∼2.4 Å from a bicarbonate oxygen.

dx.doi.org/10.1021/bi201650c | Biochemistry 2012, 51, 867−878

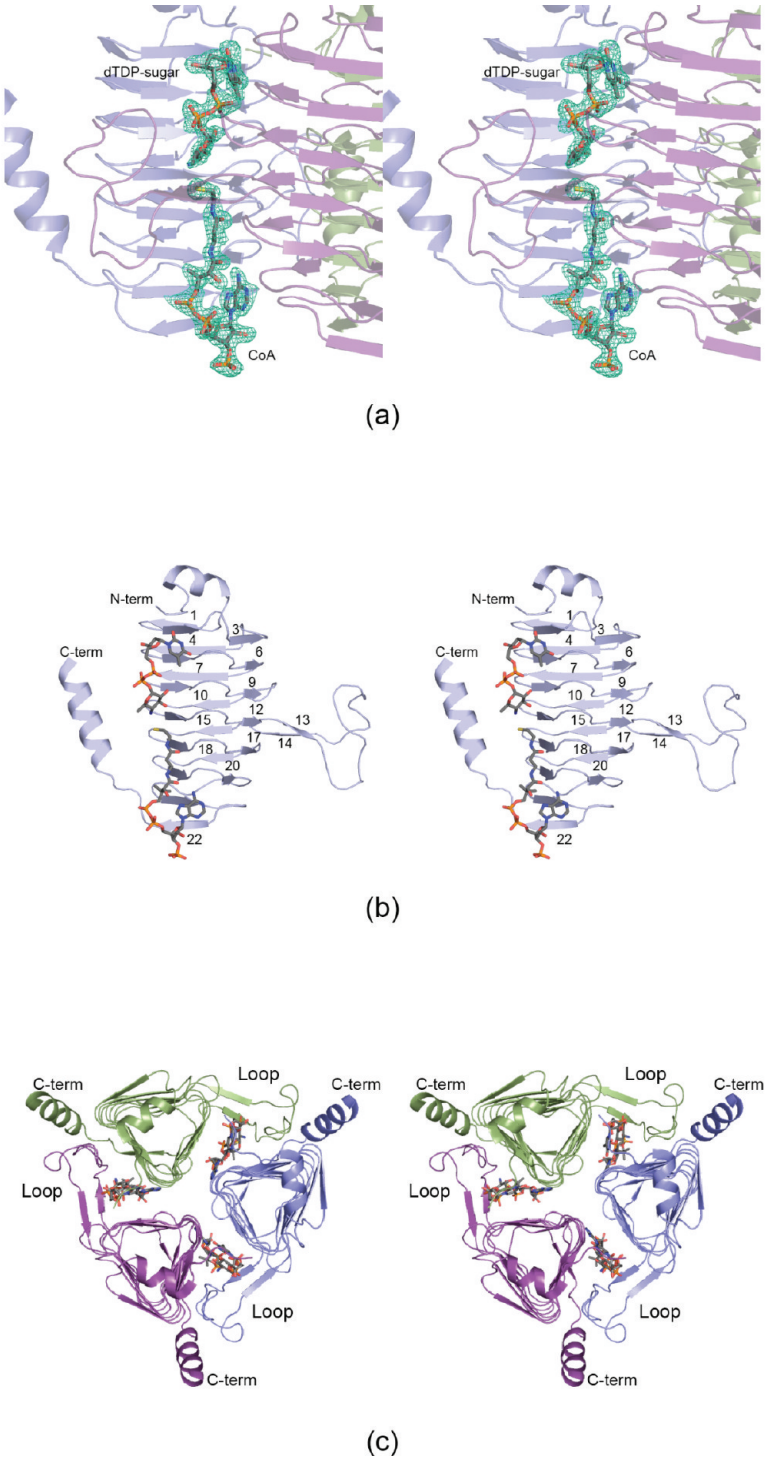

Figure 2. Structure of AntD. The first structure determined in this investigation was that of the enzyme in a complex with CoA and dTDP-4-amino-4,6-dideoxy-α-D-glucose. Shown in panel a is a portion of the electron density map corresponding to two of the bound ligands in the trimer. The map, contoured at 2.5σ, was calculated with coefficients of the form $(F_o - F_c)$, where F_o was the native structure factor amplitude, and F_c was the calculated structure factor amplitude. A ribbon representation of a single subunit of AntD is depicted in panel b, whereas the complete AntD trimer is presented in panel c. Each subunit of the trimer is highlighted in a different color, and the bound ligands are drawn as sticks. All figures were prepared with PyMOL.[33]

The natural acyl-CoA derivative used by AntD is 3-hydroxyl-3-methylbutyryl-CoA, which is commercially unavailable. It was possible to obtain β-hydroxybutyryl-CoA, however, which differs from the natural acyl-CoA substrate by the absence of a second methyl group attached to the β-carbon (Scheme 2). Thus, the second structure determined for this investgation was of a complex with the enzyme, dTDP, and β-hydroxybutyryl-CoA. The crystals diffracted to 1.8 Å resolution and also belonged to space group $P4_1$. The observed electron density corresponding to one of the bound β-hydroxybutyryl-CoA ligands in the asymmetric unit is displayed in Figure 4a. Again, the electron density map was very well ordered, and

dx.doi.org/10.1021/bi201650c | *Biochemistry* 2012, 51, 867−878

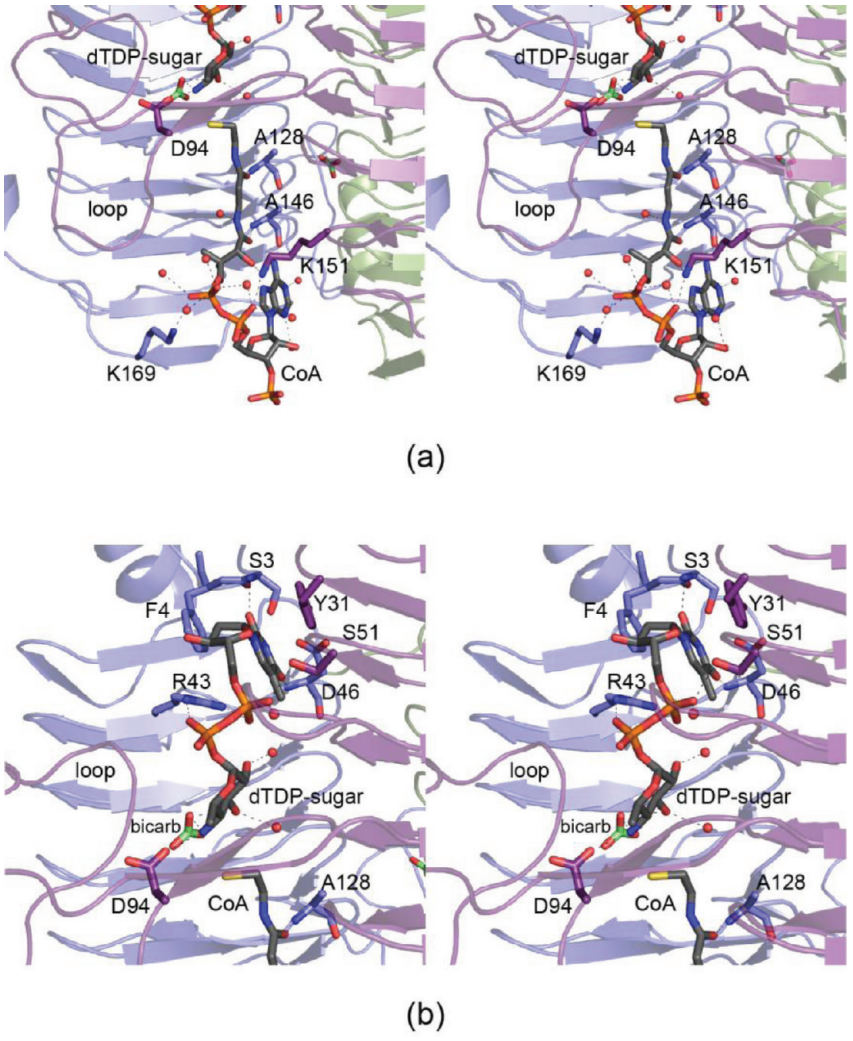

Figure 3. AntD active site. Close-up views of the regions surrounding CoA and dTDP-4-amino-4,6-dideoxy-α-D-glucose (a and b, respectively). The bicarbonate is highlighted with green bonds. Possible hydrogen bonding interactions within 3.2 Å are represented by the dashed lines. Ordered water molecules are displayed as red spheres.

the geometry for the AntD/dTDP/β-hydroxybutyryl-CoA complex model was excellent with 89.8 and 10.2% of the ϕ and ψ values lying within the core and allowed regions of the Ramachandran plot, respectively. There were no major structural changes that occurred upon the binding of β-hydroxybutyryl-CoA versus CoA. Indeed, the α-carbons for the two models superimpose with an rmsd of ~0.14 Å.

Shown in Figure 4b is a close-up view of the binding pocket for the CoA derivative. The β-hydroxybutyryl-CoA sample used in the study consisted of a D,L-mixture. On the basis of the electron density map, it was clear that the predominant form of the CoA derivative trapped in the active site had the *S*-configuration. The β-hydroxyl group of the acyl-CoA derivative interacts with a solvent molecule and the imidazole ring of His 61. It is positioned in the site occupied by the bicarbonate ion in the model of AntD with bound dTDP-sugar. Two water molecules surround the carbonyl oxygen of the acyl-CoA derivative. In addition, the hydroxyl group of Ser 84 is 3.2 Å from the acyl-CoA carbonyl oxygen. It is important to note, however, that the hydroxyl group of this serine does not lie in the correct orientation for maximal overlap between its proton and the lone pairs of electrons on the acyl-CoA carbonyl oxygen. However, during the course of the reaction, when the amino group of the dTDP-sugar attacks the acyl carbonyl carbon of CoA, the hybridization state of the carbonyl carbon changes from sp^2 to sp^3, and thus, Ser 84 may play a role in the formation of an "oxyanion hole".

It was not possible to prepare a complex of AntD with bound dTDP-4-amino-4,6-dideoxy-α-D-glucose and β-hydroxybutyryl-CoA. However, it was possible to superimpose the two models determined in this investigation together, given their close structural correspondence. As one can see in Figure 5, the sugar C-4″ amino group of the nucleotide-linked sugar is clearly in the correct orientation to attack the *si* face of the carbonyl carbon of β-hydroxybutyryl-CoA. In addition, Asp 94 is in the proper position to function as an active site base to remove the proton on the sugar amino group.

On the basis of the three-dimensional models presented here, an attractive hypothesis regarding the catalytic mechanism of AntD might be as follows. The side chain of Asp 94 serves as the active site base, and the side chain of Ser 84 stabilizes the oxyanion intermediate, which occurs as the carbonyl carbon of the acyl-CoA is attacked by the sugar amino group and becomes sp^3-hybridized. To test the possible catalytic roles of these amino acid residues in the AntD mechanism, we prepared five site-directed mutant proteins (D94N, D94A, S84A, S84T, and S84C) and determined their kinetic parameters and three-dimensional structures as described below.

dx.doi.org/10.1021/bi201650c | *Biochemistry* 2012, 51, 867−878

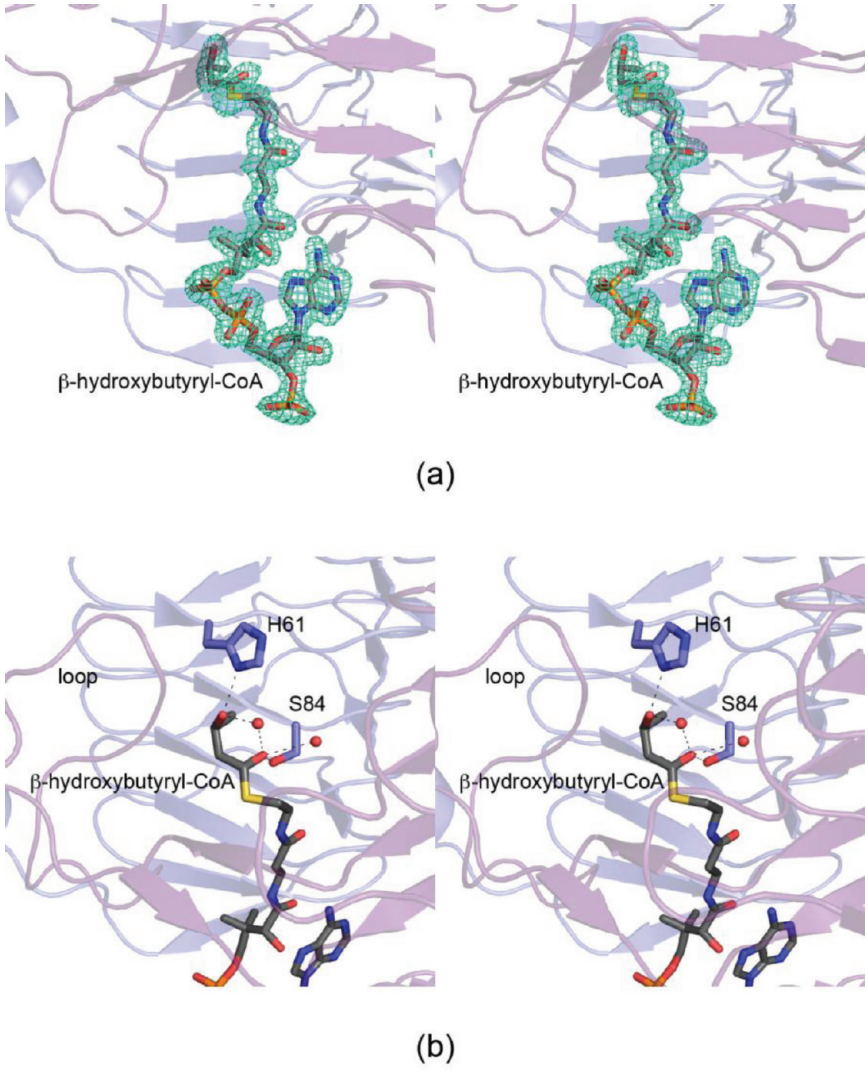

Figure 4. AntD active site with bound *β*-hydroxybutyryl-CoA. The observed electron density for one of the *β*-hydroxybutyryl-CoA ligands is shown in panel a. The map was calculated as described in the legend of Figure 2 and contoured at 3*σ*. A close-up view of the region surrounding the *β*-hydroxybutyryl moiety is presented in panel b.

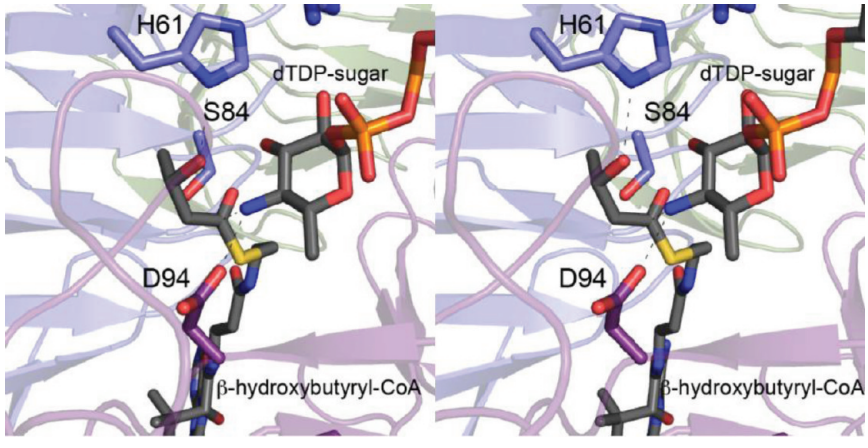

Figure 5. Active site geometry of AntD before catalysis. The dashed line between the amino nitrogen of the sugar and the carbonyl carbon of *β*-hydroxybutyryl-CoA serves to highlight the direction of nucleophilic attack. Note that the side chain of Ser 84 is ideally poised to stabilize an oxyanion tetrahedral intermediate or transition state. Asp 94 is 2.9 Å from the sugar amino group.

Kinetic and Structural Analyses of the Mutant Proteins. The first mutant protein constructed for this investigation was the D94N version of the wild-type enzyme. Its three-dimensional structure was solved to 2.3 Å resolution. Not surprisingly, the *α*-carbons for the D94N mutant protein and the wild-type enzyme corresponded with an rmsd of ~0.19 Å.

Virtually no major changes occurred in the active site upon substitution of Asp 94 with an asparagine residue. Whereas the overall molecular structure of the D94N mutant protein was unchanged, its kinetic parameters were, however, altered. Specifically, the K_m for the dTDP-sugar increased by 1 order of magnitude, the K_m for β-hydroxybutyryl-CoA increased from 0.67 to 2.3 mM, and the k_{cat}, as measured using the dTDP-sugar, decreased to ~2% of that observed for the wild-type enzyme. The catalytic efficiency of the D94N mutant protein, with respect to the dTDP-sugar substrate, decreased by approximately 4 orders of magnitude (Table 3).

The next mutant protein structure determined was the D94A version of the wild-type enzyme. Its three-dimensional structure was solved to 2.5 Å resolution. Again, there were basically no structural changes that occurred upon substitution of an alanine for an asparagine residue within experimental error except that a water molecule moved into the position normally occupied by the carboxylate side chain of Asp 94. The α-carbons for the D94A mutant protein and the wild-type enzyme were superimposed with an rmsd of ~0.22 Å. The kinetic parameters for this mutant protein were altered, however. The K_m for the dTDP-sugar increased by approximately 8-fold with respect to that of the wild-type enzyme. Strikingly, however, the K_m for β-hydroxybutyryl-CoA actually decreased by ~50%. The structural reason for this decrease in K_m is unknown. The k_{cat}, as measured using the dTDP-sugar, decreased to ~0.3% of that observed for the wild-type enzyme, and the catalytic efficiency, with respect to the dTDP-sugar substrate, was reduced by approximately 4 orders of magnitude. Importantly, however, both mutant proteins retained enzymatic activity, albeit with significantly reduced catalytic efficiencies (Table 3). These results suggest that the carboxylate group of Asp 94 is important for dTDP-sugar binding, but it probably does not function as an enzymatic base. Due to the high K_m value for the dTDP-sugars (Table 3), it was not possible to determine the structures of either the D94N or D94A mutant protein with a bound substrate. Only CoA and dTDP were observed in the electron density maps.

To test the role of Ser 84 in catalysis, three site-directed mutant proteins were prepared and studied. The first was a

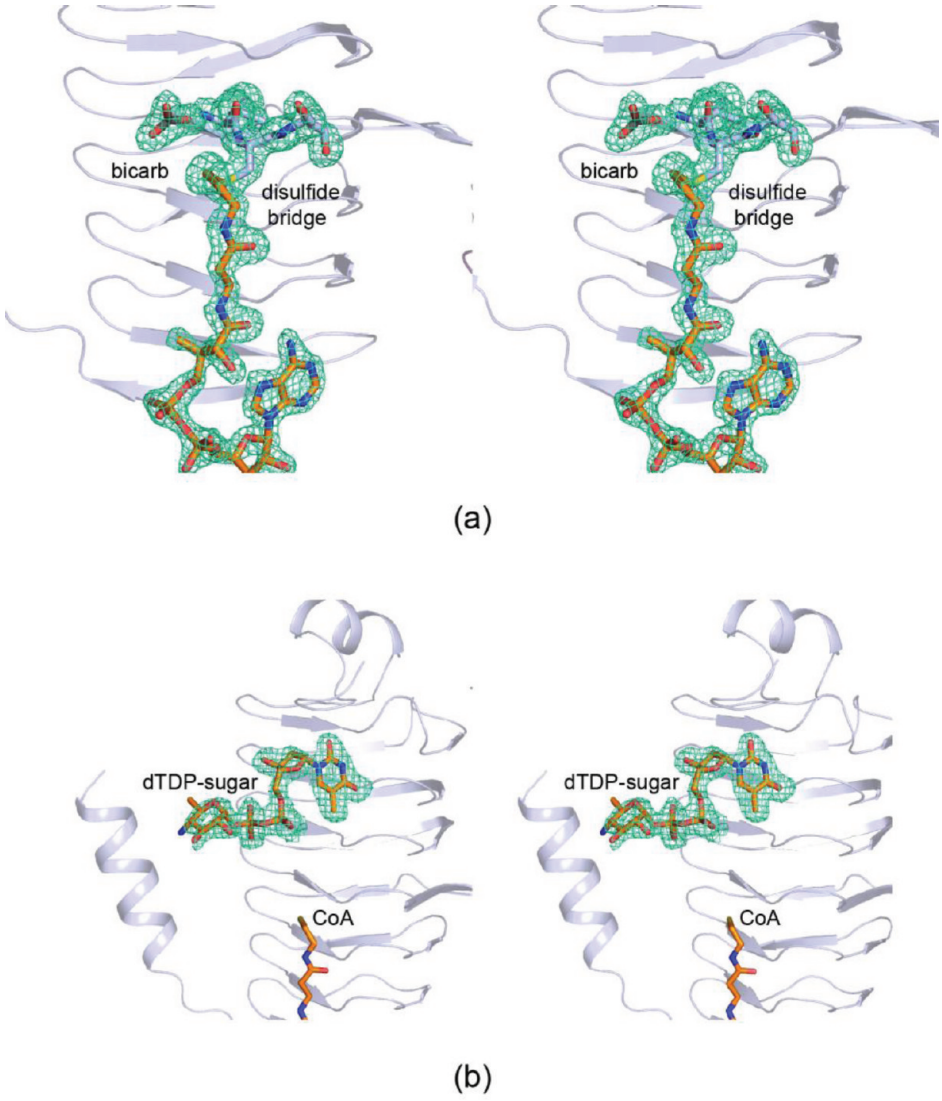

Figure 6. Electron density for the S84C mutant protein. Introduction of a cysteine residue for a serine resulted in the formation of a disulfide bond between it and the sulfur of CoA (a). The map, contoured at 3σ, was calculated with coefficients of the form $(F_o - F_c)$, where F_o was the native structure factor amplitude, and F_c was the calculated structure factor amplitude. Shown in panel b is the omit map corresponding to the dTDP-sugar. It was contoured at 2.5σ.

dx.doi.org/10.1021/bi201650c | *Biochemistry* 2012, 51, 867–878

Scheme 3

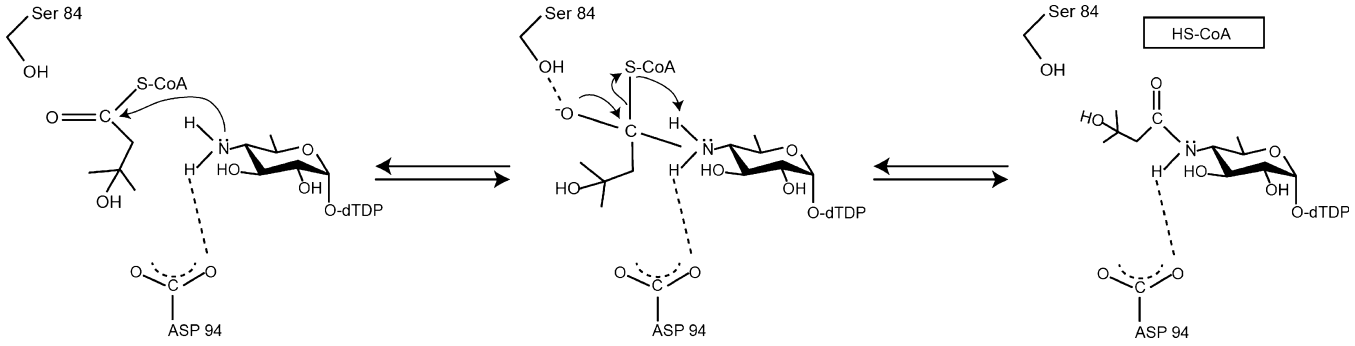

mutant protein in which Ser 84 was changed to an alanine residue. For this protein, the K_m for the dTDP-sugar remained the same as that exhibited by the wild-type enzyme, whereas its K_m for β-hydroxybutyryl-CoA was reduced by ~25%. The k_{cat} values, with respect to those of both the dTDP-sugar and the β-hydroxybutyryl-CoA, were reduced by ~1 order of magnitude from that observed for the wild-type enzyme (Table 3). The catalytic efficiency with respect to the dTDP-sugar was also reduced by 1 order of magnitude. To ensure that the observed differences in kinetic parameters between the wild-type enzyme and the S84A mutant protein were not due to major conformational changes, the three-dimensional structure of the S84A mutant protein was subsequently determined to 2.2 Å resolution. The dTDP-sugar and the CoA were observed binding in the active site pocket. Within experimental error, the wild-type and S84A mutant proteins are virtually identical with respect to their three-dimensional architectures. Indeed, their α-carbons superimpose with an rmsd of 0.12 Å. Thus, the reduction in catalytic efficiency for the S84A mutant protein is simply due to the loss of a hydroxyl group rather than a major conformational perturbation.

To further test the role of a hydroxyl group at position 84, two additional mutant proteins were prepared: S84T and S84C. The S84T mutant protein exhibited kinetic parameters similar to those measured for the S84A version, whereas the S84C mutant protein showed a 50% decrease in K_m for the dTDP-sugar when compared to that of the wild-type enzyme (Table 3). Unexpectedly, both the S84T and S84C mutant proteins demonstrated substrate inhibition with the dTDP-sugar, and thus, it was not possible to determine their kinetic parameters with respect to β-hydroxybutyryl-CoA.

We were curious about why these two mutant proteins demonstrated substrate inhibition with respect to the dTDP-sugar, and thus, their X-ray structures were solved. For the S84T mutant protein, X-ray data were collected to 1.9 Å resolution. The electron density for the bicarbonate was unambiguous, whereas that for the dTDP-sugar was less convincing. The dTDP moiety of the nucleotide-linked sugar was absolutely clear, but the hexose moiety was weak and appeared to be oriented toward the solvent rather than directed toward the sulfhydryl group of CoA. In addition, there was residual $F_o - F_c$ electron density around the threonine residue at position 84, suggesting that multiple conformations for the side chain were occurring. The α-carbons for the wild-type and S84T mutant proteins correspond with an rmsd of 0.14 Å.

The S84C mutant protein structure was less ambiguous. Crystals of this mutant protein also diffracted to 1.9 Å resolution. Surprisingly, a disulfide bond formed between the sulfhydryl group of CoA and the cysteine, which can be seen in the electron density map in Figure 6a. The disulfide bond adopts a left-handed spiral with the sulfur atoms separated by ~2.0 Å. The bicarbonate ion is located near the disulfide bridge (Figure 6a). The electron density corresponding to the dTDP-sugar was also unambiguous and showed that the pyranosyl moiety of the substrate was directed out of the active site pocket rather than toward the CoA (Figure 6b). Most likely, the observed substrate inhibition observed with the S84T and S84C mutant enzymes arose primarily as a result of this alternative sugar binding mode. Clearly, introduction of a more bulky threonine or cysteine residue at position 84, and in the case of the S84C mutant protein, the formation of a disulfide bridge perturbed the active site enough to allow for this alternative dTDP-sugar binding conformation. Due to the high cost of β-hydroxybutyryl-CoA, we could not determine the mechanism of substrate inhibition for these two mutant proteins, but most likely it is competitive.

Conclusions. Taken together, the combined site-directed mutagenesis, kinetic, and X-ray crystallographic analyses of AntD suggest that the primary function of Asp 94 is to anchor the dTDP-sugar into the active site, and that Ser 84, although not absolutely required for catalysis, most likely plays a role in stabilization of the oxyanion intermediate. The question of how the proton on the sugar amino group is removed during the acylation process then arises. Clues to this question come from the recent biochemical and X-ray crystallographic studies of QdtC and WlbB, *N*-acetyltransferases involved in the biosynthesis of unusual acetamido sugars.[19,20] Like AntD, these enzymes adopt left-handed β-helix architectures, and both enzymes lack an active site base. On the basis of detailed structural and functional studies, it has been proposed that catalysis by QdtC and WlbB occurs via a substrate-assisted mechanism, or in other words, the sulfur of CoA ultimately functions as the base to remove the amino proton. In light of these studies, a possible catalytic mechanism for AntD is shown in Scheme 3. The proposed mechanism assumes that the amino group of the sugar binds in the active site in the unprotonated state and that the pK_a of the CoA sulfur is perturbed enough so that the sulfur functions as a base. Quantum and molecular mechanical studies may shed light on whether the proposed mechanism is thermodynamically and chemically feasible. These studies are presently underway.

It has become increasingly apparent within recent years that unusual sugars play important roles in the efficacies of natural compounds such as erythromycin, an antibiotic,[31] and doxorubicin, an antitumor agent.[32] Indeed, it is well-established that the carbohydrate substituents are important for proper binding of such compounds, and it has been shown that the aglycone of doxorubicin alone, for example, is nearly inactive

dx.doi.org/10.1021/bi201650c | *Biochemistry* 2012, 51, 867−878

when tested for anticancer activity.[32] The biochemical analysis of AntD presented here provides a molecular foundation for ultimately preparing on a large-scale basis unique acylated sugars through the judicious use of site-directed mutant versions of AntD and various acylated CoAs.

■ ASSOCIATED CONTENT

Accession Codes

X-ray coordinates have been deposited in the Protein Data Bank as entries 3VBI, 3VBJ, 3VBK, 3VBL, 3VBM, 3VBN, and 3VBP.

■ AUTHOR INFORMATION

Corresponding Author

*E-mail: hazel_holden@biochem.wisc.edu. Fax: (608) 262-1319. Phone: (608) 262-4988.

Funding

This research was supported in part by National Science Foundation (NSF) Grant MCB-0849274 to H.M.H. and NSF Predoctoral Fellowship DGE-0718123 to R.L.K.

Notes

The authors have no competing financial or other interests.

■ ACKNOWLEDGMENTS

We are grateful to the students of Project CRYSTAL for growing the first crystals of AntD (http://www.projectcrystal.org/). We thank Molly McDevitt and Matthew Zmudka for help with the cloning and crystallizations of several AntD mutant proteins. We gratefully acknowledge Dr. James B. Thoden and Mr. Nathan Bruender for helpful discussions. Finally, we thank Professor Grover Waldrop for critically reading the manuscript.

■ ABBREVIATIONS

CoA, coenzyme A; ESI, electrospray ionization; HEPES, *N*-(2-hydroxyethyl)piperazine-*N*′-2-ethanesulfonic acid; PCR, polymerase chain reaction; PLP, pyridoxal 5′-phosphate; rmsd, root-mean-square deviation; dTDP, thymidine 5′-diphosphate; TEV, tobacco etch virus.

■ REFERENCES

(1) Takamatsu, H., and Watabe, K. (2002) Assembly and genetics of spore protective structures. *Cell. Mol. Life Sci. 59*, 434−444.

(2) Dixon, T. C., Meselson, M., Guillemin, J., and Hanna, P. C. (1999) Anthrax. *N. Engl. J. Med. 341*, 815−826.

(3) Steichen, C., Chen, P., Kearney, J. F., and Turnbough, C. L. Jr. (2003) Identification of the immunodominant protein and other proteins of the *Bacillus anthracis* exosporium. *J. Bacteriol. 185*, 1903−1910.

(4) Redmond, C., Baillie, L. W., Hibbs, S., Moir, A. J., and Moir, A. (2004) Identification of proteins in the exosporium of *Bacillus anthracis*. *Microbiology 150*, 355−363.

(5) Matz, L. L., Beaman, T. C., and Gerhardt, P. (1970) Chemical composition of exosporium from spores of *Bacillus cereus*. *J. Bacteriol. 101*, 196−201.

(6) Todd, S. J., Moir, A. J., Johnson, M. J., and Moir, A. (2003) Genes of *Bacillus cereus* and *Bacillus anthracis* encoding proteins of the exosporium. *J. Bacteriol. 185*, 3373−3378.

(7) Williams, D. D., and Turnbough, C. L. Jr. (2004) Surface layer protein EA1 is not a component of *Bacillus anthracis* spores but is a persistent contaminant in spore preparations. *J. Bacteriol. 186*, 566−569.

(8) Sylvestre, P., Couture-Tosi, E., and Mock, M. (2002) A collagen-like surface glycoprotein is a structural component of the *Bacillus anthracis* exosporium. *Mol. Microbiol. 45*, 169−178.

(9) Sylvestre, P., Couture-Tosi, E., and Mock, M. (2003) Polymorphism in the collagen-like region of the *Bacillus anthracis* BclA protein leads to variation in exosporium filament length. *J. Bacteriol. 185*, 1555−1563.

(10) Daubenspeck, J. M., Zeng, H., Chen, P., Dong, S., Steichen, C. T., Krishna, N. R., Pritchard, D. G., and Turnbough, C. L. Jr. (2004) Novel oligosaccharide side chains of the collagen-like region of BclA, the major glycoprotein of the *Bacillus anthracis* exosporium. *J. Biol. Chem. 279*, 30945−30953.

(11) Dong, S., McPherson, S. A., Tan, L., Chesnokova, O. N., Turnbough, C. L. Jr., and Pritchard, D. G. (2008) Anthrose biosynthetic operon of *Bacillus anthracis*. *J. Bacteriol. 190*, 2350−2359.

(12) Kuehn, A., Kovac, P., Saksena, R., Bannert, N., Klee, S. R., Ranisch, H., and Grunow, R. (2009) Development of antibodies against anthrose tetrasaccharide for specific detection of *Bacillus anthracis* spores. *Clin. Vaccine Immunol. 16*, 1728−1737.

(13) Fujiwara, N., Nakata, N., Maeda, S., Naka, T., Doe, M., Yano, I., and Kobayashi, K. (2007) Structural characterization of a specific glycopeptidolipid containing a novel *N*-acyl-deoxy sugar from *Mycobacterium* intracellulare serotype 7 and genetic analysis of its glycosylation pathway. *J. Bacteriol. 189*, 1099−1108.

(14) Kubler-Kielb, J., Vinogradov, E., Hu, H., Leppla, S. H., Robbins, J. B., and Schneerson, R. (2008) Saccharides cross-reactive with *Bacillus anthracis* spore glycoprotein as an anthrax vaccine component. *Proc. Natl. Acad. Sci. U.S.A. 105*, 8709−8712.

(15) Dong, S., McPherson, S. A., Wang, Y., Li, M., Wang, P., Turnbough, C. L. Jr., and Pritchard, D. G. (2010) Characterization of the enzymes encoded by the anthrose biosynthetic operon of *Bacillus anthracis*. *J. Bacteriol. 192*, 5053−5062.

(16) Raetz, C. R., and Roderick, S. L. (1995) A left-handed parallel β helix in the structure of UDP-*N*-acetylglucosamine acyltransferase. *Science 270*, 997−1000.

(17) Rangarajan, E. S., Ruane, K. M., Sulea, T., Watson, D. C., Proteau, A., Leclerc, S., Cygler, M., Matte, A., and Young, N. M. (2008) Structure and active site residues of PglD, an *N*-acetyltransferase from the bacillosamine synthetic pathway required for *N*-glycan synthesis in *Campylobacter jejuni*. *Biochemistry 47*, 1827−1836.

(18) Olivier, N. B., and Imperiali, B. (2008) Crystal structure and catalytic mechanism of PglD from *Campylobacter jejuni*. *J. Biol. Chem. 283*, 27937−27946.

(19) Thoden, J. B., Cook, P. D., Schaffer, C., Messner, P., and Holden, H. M. (2009) Structural and functional studies of QdtC: An *N*-acetyltransferase required for the biosynthesis of dTDP-3-acetamido-3,6-dideoxy-α-D-glucose. *Biochemistry 48*, 2699−2709.

(20) Thoden, J. B., and Holden, H. M. (2010) Molecular structure of WlbB, a bacterial *N*-acetyltransferase involved in the biosynthesis of 2,3-diacetamido-2,3-dideoxy-D-mannuronic acid. *Biochemistry 49*, 4644−4653.

(21) Thoden, J. B., Timson, D. J., Reece, R. J., and Holden, H. M. (2005) Molecular structure of human galactokinase: implications for Type II galactosemia. *J. Biol. Chem. 280*, 9662−9670.

(22) Burgie, E. S., and Holden, H. M. (2007) Molecular architecture of DesI: A key enzyme in the biosynthesis of desosamine. *Biochemistry 46*, 8999−9006.

(23) Terwilliger, T. C., and Berendzen, J. (1999) Automated MAD and MIR structure solution. *Acta Crystallogr. D55* (Part 4), 849−861.

(24) Terwilliger, T. C. (2000) Maximum-likelihood density modification. *Acta Crystallogr. D56* (Part 8), 965−972.

(25) Emsley, P., and Cowtan, K. (2004) Coot: Model-building tools for molecular graphics. *Acta Crystallogr. D60*, 2126−2132.

(26) Murshudov, G. N., Vagin, A. A., and Dodson, E. J. (1997) Refinement of macromolecular structures by the maximum-likelihood method. *Acta Crystallogr. D53*, 240−255.

(27) McCoy, A. J., Grosse-Kunstleve, R. W., Adams, P. D., Winn, M. D., Storoni, L. C., and Read, R. J. (2007) Phaser crystallographic software. *J. Appl. Crystallogr. 40*, 658−674.

(28) Alpers, D. H., Appel, S. H., and Tomkins, G. M. (1965) A spectrophotometric assay for thiogalactoside transacetylase. *J. Biol. Chem. 240*, 10−13.
(29) Magalhaes, M. L., and Blanchard, J. S. (2005) The kinetic mechanism of AAC3-IV aminoglycoside acetyltransferase from *Escherichia coli*. *Biochemistry 44*, 16275−16283.
(30) Laskowski, R. A., MacArthur, M. W., Moss, D. S., and Thornton, J. M. (1993) *PROCHECK*: A program to check the stereochemical quality of protein structures. *J. Appl. Crystallogr. 26*, 283−291.
(31) Weymouth-Wilson, A. C. (1997) The role of carbohydrates in biologically active natural products. *Nat. Prod. Rep. 14*, 99−110.
(32) Zhu, L., Cao, X., Chen, W., Zhang, G., Sun, D., and Wang, P. G. (2005) Syntheses and biological activities of daunorubicin analogs with uncommon sugars. *Bioorg. Med. Chem. 13*, 6381−6387.
(33) DeLano, W. L. (2002) *The PyMOL Molecular Graphics System*, DeLano Scientific, San Carlos, CA.